International Journal of Pharmacology

Int. J. Pharmacol. **2026**; 22(2): 46622
https://doi.org/10.31083/IJP46622

Research Article

The Effect of Danshen on Fibrosis and Iron Metabolism in a Rat Model of Hepatic Fibrosis

Wuying Ou[1], Chunyun Li[1,*]

[1]Clinical Laboratory, Haikou Affiliated Hospital of Central South University XiangYa School of Medicine, 270208 Haikou, Hainan, China
*Correspondence: lichunyun98628@163.com (Chunyun Li)

Academic Editor: Mehmet Ozaslan
Submitted: 16 September 2025 Revised: 14 December 2025 Accepted: 29 December 2025 Published: 24 April 2026

Abstract

Background: Hepatic fibrosis (HF) is a major global health burden with limited effective therapies. Ferroptosis, an iron-dependent form of cell death, and inflammatory pathways are implicated in HF progression. Salvia miltiorrhiza (Danshen) has demonstrated antifibrotic effects, but its underlying mechanisms remain unclear. **Objective**: To elucidate the mechanisms of Danshen in treating HF through network pharmacology and experimental validation, focusing on the JAK/STAT pathway, iron metabolism, and ferroptosis. **Methods**: Using the Traditional Chinese Medicine Systems Pharmacology (TCMSP) database, we identified 92 common targets among Danshen components, HF-related genes, and iron metabolism genes. A CCl_4-induced HF rat model was established (n = 70) and treated with Danshen (3 or 6 g/kg/d) for 4 weeks. Hepatic fibrosis was assessed by Masson staining. Serum markers including Fe^{2+}, transferrin (TRF), ferritin (SF), type III procollagen (PCIII), hydroxyproline (HyP), malondialdehyde (MDA), and glutathione (GSH) were measured. Western blotting evaluated hepatic expression of IL-6, P-JAK2, p-STAT3, and GPX4. **Results**: Network pharmacology revealed JAK2/STAT3 as top hub genes among 92 intersection targets. High-dose Danshen decreased IL-6, P-JAK2, and p-STAT3 expression by 45–60% ($p < 0.05$), increased serum Fe^{2+} and TRF by 1.8-fold, and reduced SF, HyP by >40% and PCIII by >15% ($p < 0.05$). Additionally, Danshen restored GPX4 protein expression and suppressed ferroptosis by decreasing MDA while increasing GSH ($p < 0.01$). Masson staining showed 55% reduction in collagen deposition with high-dose treatment. **Conclusion**: Danshen alleviates hepatic fibrosis by modulating the JAK/STAT-iron-ferroptosis axis, establishing a novel multi-target therapeutic strategy for HF.

Keywords: Danshen; liver fibrosis ferroptosis; iron metabolism disorders; network pharmacology

1. Introduction

Hepatic fibrosis (HF) is a disease characterized by abnormal activation of hepatic stellate cells, an imbalance between the synthesis and degradation of extracellular matrix proteins, and excessive deposition that disrupts the normal structure of the liver resulting from various chronic liver injuries [1]. The global incidence rate of HF is between 4.5% and 9.0%. Liver injury first occurs during the progression of HF [2]. As injury accumulates, the body initially activates pro-inflammatory mechanisms. With the onset of inflammatory responses, the normal structure and physiological functions of liver tissue are gradually disrupted, leading to scar tissue formation and fibrosis [3]. As the degree of HF worsens, it can progress to irreversible cirrhosis and hepatocellular carcinoma, posing a significant challenge to global health [4].

Ferroptosis is a newly discovered form of iron-dependent cell death that has been studied in recent years, primarily involving abnormal iron ion metabolism, accumulation of lipid peroxides, and weakening of the antioxidant defense system. Numerous studies have indicated that inducing ferroptosis in hepatic stellate cells (HSCs) or alleviating ferroptosis in the liver can improve HF and reduce liver damage [5]. The central link in HF is the activation of HSCs; other liver cells also influence HSC activation [6]. In the pathological states of liver injury, ferroptosis affects multiple liver cell types and accelerates the progression of HF [7].

Currently, there is a lack of effective drugs for the treatment of HF in clinical practice. With the widespread application of traditional Chinese medicine (TCM) in various chronic liver diseases, its advantages such as fewer side effects, high safety, and the unique characteristics of being comprehensive and multi-targeted have gradually emerged [8]. Compared with Western medicine, TCM has unique advantages in the treatment of chronic diseases and can effectively reverse HF. However, the specific mechanisms of action are not yet fully understood and require further exploration [9]. Therefore, researching effective new diagnostic and treatment methods for HF is significant and of economic value.

Salvia miltiorrhiza, commonly known as Danshen, is known for its effects and functions such as promoting blood circulation to remove blood stasis, reducing liver inflammation, inhibiting the proliferation of hepatic stellate cells, improving liver function, and anti-HF [10]. This study aimed to construct a rat model of HF by injecting a mixture of carbon tetrachloride and vegetable oil into the main limbs of rats to provide scientific evidence for the treatment of HF with Danshen. Additionally, this study will combine

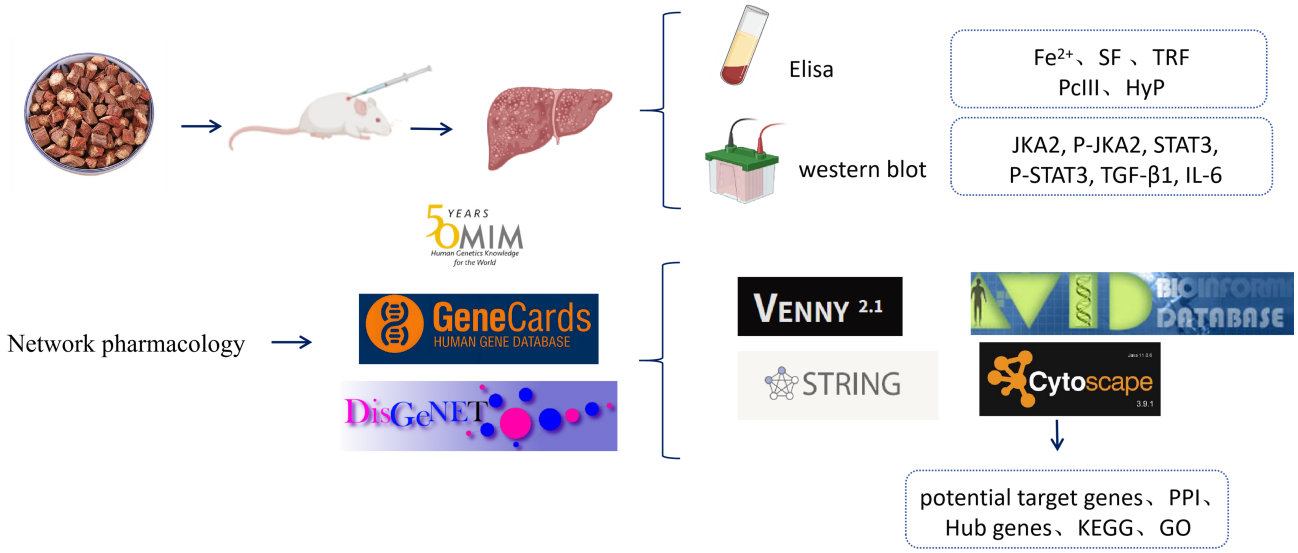

Fig. 1. Detailed design flow chart of the current study. Created in BioRender. https://BioRender.com/al17dt9.

network pharmacology methods to identify the main active components of Danshen and further analyze its potential targets and mechanisms in anti-HF (Fig. 1).

2. Materials and Methods

2.1 Animals

Sibe Biotechnology Co., Ltd. (Beijing) provided 70 SPF-grade male Sprague-Dawley (SD) rats, weighing (200 ± 20) g, with license number SCXK (Beijing) 2019-0010. All rats were housed in a feeding room at a temperature of 22–25 °C and humidity of 50%–65%, with free access to food and water. This study was approved by the Biomedical Ethics Committee of the Haikou Affiliated Hospital of Central South University XiangYa School of Medicine (i.e., Haikou people's Hospital).

2.2 Drugs and Reagents

Danshen was purchased from Guangdong Yifang Pharmaceutical Co., Ltd. (Foshan, Guangdong, China), Masson (Macklin-M774677), and paraformaldehyde (Macklin-P885233) were purchased from Shanghai Macklin Biochemical Technology Co., Ltd. (Shanghai, China); β-actin Antibody (1:1000, AF7018, Affinity, Cincinnati, OH, USA), JAK2 Antibody (1:1000, AF6022, Affinity, Cincinnati, OH, USA), Phospho-JAK2 Antibody (1:1000, AF3024, Affinity, Cincinnati, OH, USA), STAT3 Antibody (1:1000, AF6294, Affinity, Cincinnati, OH, USA), Phospho-STAT3Antibody (1:1000, AF3293, Affinity, Cincinnati, OH, USA), TGF-β1 Antibody (1:1000, AF1027, Affinity, Cincinnati, OH, USA), IL-6 Antibody (1:1000, DF6087, Affinity, Cincinnati, OH, USA) and Goat Anti-Rabbit IgG (H+L) HRP (1:5000, S0001, Affinity, Cincinnati, OH, USA) were purchased from Affinity Biosciences LTD (Shanghai, China); ELISA kits: Serum iron determination kit Fe^{2+} (colorimetric method) A039-1-1, Ferritin SF test kit H129-1-1, Transferrin (TRF) test kit H130-1-1, Type III procollagen (PCIII) reagent kit H212-1-1, Hydroxyproline (Hyp) determination reagent kit (alkaline hydrolysis method) A030-2-1 were purchased from Nanjing Jianchen Bioengineering Institute (Nanjing, Jiangsu, China).

2.3 Grouping, Model Establishment, and Drug Administration

After a 1-week acclimatization period, 70 male SD rats were randomly assigned to four groups using a random number table: a normal control group with 10 rats, a model group with 20 rats, and two Danshen treatment groups with 20 rats each receiving low (3 $g \cdot kg^{-1} \cdot d^{-1}$) and high (6 $g \cdot kg^{-1} \cdot d^{-1}$) doses of Danshen. Except for the normal control group, the other three groups were alternately given a subcutaneous injection of a carbon tetrachloride-vegetable oil mixture on the inner side of the limbs, at a dosage of 0.3 mL/100 g body weight, twice a week. To observe the appearance of the liver and assess the degree of HF, rats were anesthetized via intramuscular injection of Zoletil 50 (Tiletamine - zolazepam composite anesthetic, 50 mg/kg) and sacrificed at 1, 4, and 8 weeks after the initial injection. Euthanasia was performed by cervical dislocation while the rats were under deep anesthesia. The successful establishment of the HF model was confirmed by histopathological examination of liver tissue sections stained with hematoxylin and eosin (HE). On day 9, the Danshen low- and high-dose groups began treatment with daily administration for a continuous period of 4 weeks.

2.4 Danshen Compound and Target Selection

Search for "Danshen" in the Traditional Chinese Medicine Systems Pharmacology Database (TCMSP, https://tcmsp-e.com/), and set the Absorption, Distribu-

tion, Metabolism, Excretion (ADME) parameters with OB $\geq$30% and DL $\geq$0.18 as the screening criteria to select the pharmacologically active compounds of Danshen. The TCMSP database was used to identify the corresponding target proteins for these compounds. Next, we used the STRING database (http://www.string-db.org) to filter by species and convert the target protein names to "gene symbol" notation.

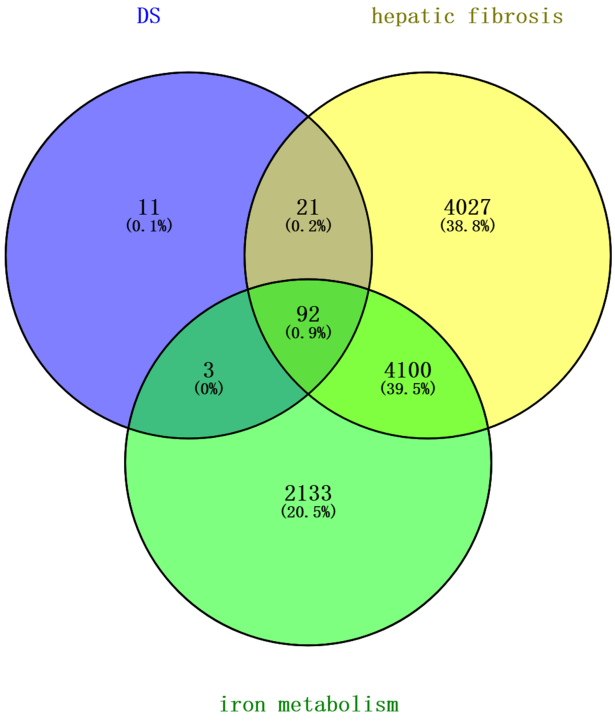

Fig. 2. Venn diagram of targets related to Danshen and HF and iron metabolism. HF, Hepatic fibrosis.

2.5 Disease-Related Target Selection

Using "HF" and "iron metabolism" as search terms, disease targets were identified using the GeneCards database (https://www.genecards.org/), and Venn diagrams were used to identify the common targets of the two diseases.

2.6 Danshen's Potential Targets for the Treatment of HF and Iron Metabolism Prediction

Translate the main pharmacological components, targets, and corresponding target genes related to diseases of Danshen into Venny 2.1 (http://bioinfogp.cnb.csic.es/tools/venny/index.html), which are potential target genes for Danshen in the treatment of HF and iron metabolism.

2.7 Core Target Screening and Network Construction

Import the obtained common target genes into the STRING database, select the species "Homo sapiens", and set the minimum interaction score to the highest confidence level of 0.40. We then obtained an overlapping gene Protein-Protein Interaction (PPI) network diagram. The PPI network diagram was imported into Cytoscape 3.9.1 software (San Francisco, CA, USA), and the maximum clique centrality (MCC) algorithm in the cytoHubba plugin was used to identify the top ten most significant hub genes.

2.8 GO and KEGG Pathway Enrichment Analysis

Utilize The DAVID database (http://david.abcc.ncifcrf.gov) was used to perform Gene Ontology (GO) functional analysis and Kyoto Encyclopedia of Genes and Genomes (KEGG) pathway enrichment for the common targets of Danshen in the treatment of HF and iron metabolism, thereby obtaining biological processes (BP), cellular components (CC), molecular functions (MF), and signaling pathways that are closely associated with the therapeutic effects of Danshen on HF and iron metabolism.

2.9 Observation of the Therapeutic Effect of Danshen on Liver Tissue Fibrosis Under a Light Microscope After Masson Staining

Liver tissues were taken from each group of rats, fixed with formaldehyde, and paraffin sections were prepared. The sections were dewaxed routinely. The sections were stained with hematoxylin for 10 min. The mixture was rinsed with distilled water three times. The sections were stained with Masson's trichrome and picric acid for 30 min. Differentiate and dehydrate directly with anhydrous alcohol and mount with neutral resin. Images were obtained under a microscope to assess the degree of HF.

2.10 Determination of Indices for Danshen Treatment of HF

Rat liver tissue was used to detect the protein expression of IL-6, JAK, and STAT by western blotting. Lysis buffer was added to extract proteins, homogenized, and centrifuged, and the total protein concentration was measured with the BCA method, boiled, loaded samples, transferred to a membrane, and blocked; diluted mouse-sourced IL-6 (1:500), JAK (1:500), STAT3 (1:500), and β-actin (1:2000) primary antibodies were incubated overnight at 4 °C; goat anti-mouse secondary antibody (1:2000) was added and incubated at 37 °C for 2 h, washed and added to the developing solution, and developed and photographed in the imaging instrument, using β-actin as an internal control to calculate the relative expression levels of the proteins.

2.11 Determination of Blood Iron Metabolism Indicators

Orbital venous blood was collected from the rats, centrifuged at 3000 rpm for 10–15 minutes to separate the serum, and then centrifuged again at 3000 rpm for 5 min. Fe^{2+}, TRF, and ferritin levels were detected according to the instructions of the ELISA kit.

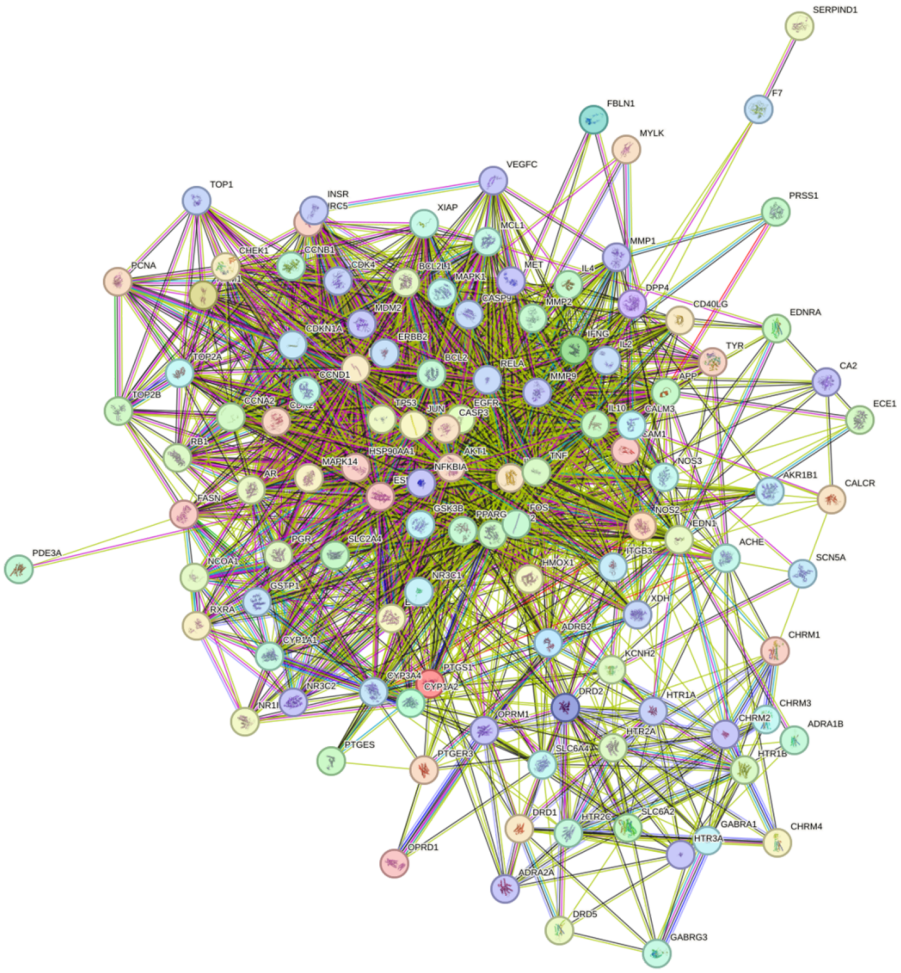

Fig. 3. PPI network of Danshen in the treatment of HF and iron metabolism. PPI, Protein-Protein Interaction.

2.12 Statistical Analysis

Graph Pad Prism software (version 9.0, Boston, MA, USA) was used for the data processing. All data were expressed as mean ± standard deviation (mean ± SD). For comparisons between two groups, the *t*-test was used, and for comparisons among multiple groups, one-way Analysis of Variance (ANOVA) was used.

3. Results

3.1 The Main Pharmacologically Active Compounds and Target Genes of Danshen (Salvia miltiorrhiza)

By querying the TCMSP database, we obtained 20 pharmacologically active compounds from Danshen and their corresponding 188 targets. Information regarding the main pharmacologically active compounds is presented in Table 1.

3.2 Mining of Targets for Danshen in the Treatment of HF and Iron Metabolism

After mapping the targets corresponding to Danshen's active compounds, targets corresponding to HF, and targets corresponding to iron metabolism using a Venn diagram, 92 common targets were identified (Fig. 2).

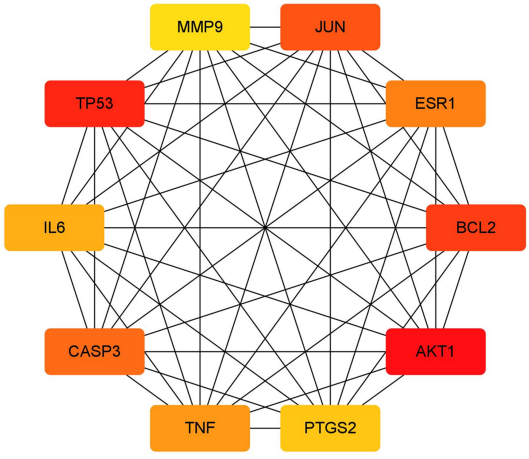

Fig. 4. Top 10 hub genes in the treatment of HF and iron metabolism by Danshen.

Table 1. Main pharmacologically active compounds of Danshen and their corresponding ADME parameters.

MOL ID	NAME	OB	DL
MOL001601	1,2,5,6-tetrahydrotanshinone	38.75	0.36
MOL001659	Poriferasterol	43.83	0.76
MOL001771	poriferast-5-en-3beta-ol	36.91	0.75
MOL001942	isoimperatorin	45.46	0.23
MOL002222	sugiol	36.11	0.28
MOL002651	Dehydrotanshinone II A	43.76	0.4
MOL002776	Baicalin	40.12	0.75
MOL000569	digallate	61.85	0.26
MOL000006	luteolin	36.16	0.25
MOL006824	alpha-amyrin	39.51	0.76
MOL007036	5,6-dihydroxy-7-isopropyl-1,1-dimethyl-2,3-dihydrophenanthren-4-one	33.77	0.29
MOL007041	2-isopropyl-8-methylphenanthrene-3,4-dione	40.86	0.23
MOL007045	3α-hydroxytanshinoneIIa	44.93	0.44
MOL007048	(E)-3-[2-(3,4-dihydroxyphenyl)-7-hydroxy-benzofuran-4-yl]acrylic acid	48.24	0.31
MOL007049	4-methylenemiltirone	34.35	0.23
MOL007050	2-(4-hydroxy-3-methoxyphenyl)-5-(3-hydroxypropyl)-7-methoxy-3-benzofurancarboxaldehyde	62.78	0.4
MOL007051	6-o-syringyl-8-o-acetyl shanzhiside methyl ester	46.69	0.71
MOL007058	formyltanshinone	73.44	0.42
MOL007059	3-beta-Hydroxymethyllenetanshiquinone	32.16	0.41
MOL007061	Methylenetanshinquinone	37.07	0.36
MOL007063	przewalskin a	37.11	0.65
MOL007064	przewalskin b	110.32	0.44
MOL007068	Przewaquinone B	62.24	0.41
MOL007069	przewaquinone c	55.74	0.4
MOL007070	(6S,7R)-6,7-dihydroxy-1,6-dimethyl-8,9-dihydro-7H-naphtho[8,7-g]benzofuran-10,11-dione	41.31	0.45
MOL007071	przewaquinone f	40.31	0.46
MOL007077	sclareol	43.67	0.21
MOL007079	tanshinaldehyde	52.47	0.45
MOL007081	Danshenol B	57.95	0.56
MOL007082	Danshenol A	56.97	0.52
MOL007085	Salvilenone	30.38	0.38
MOL007088	cryptotanshinone	52.34	0.4
MOL007093	dan-shexinkum d	38.88	0.55
MOL007094	danshenspiroketallactone	50.43	0.31
MOL007098	deoxyneocryptotanshinone	49.4	0.29
MOL007100	dihydrotanshinlactone	38.68	0.32
MOL007101	dihydrotanshinoneI	45.04	0.36
MOL007105	epidanshenspiroketallactone	68.27	0.31
MOL007107	C09092	36.07	0.25
MOL007108	isocryptotanshi-none	54.98	0.39
MOL007111	Isotanshinone II	49.92	0.4
MOL007115	manool	45.04	0.2
MOL007118	microstegiol	39.61	0.28
MOL007119	miltionone I	49.68	0.32
MOL007120	miltionone II	71.03	0.44
MOL007121	miltipolone	36.56	0.37
MOL007122	Miltirone	38.76	0.25
MOL007123	miltirone II	44.95	0.24
MOL007124	neocryptotanshinone ii	39.46	0.23
MOL007125	neocryptotanshinone	52.49	0.32
MOL007127	1-methyl-8,9-dihydro-7H-naphtho[5,6-g]benzofuran-6,10,11-trione	34.72	0.37
MOL007130	prolithospermic acid	64.37	0.31

Table 1. Continued.

MOL ID	NAME	OB	DL
MOL007132	(2R)-3-(3,4-dihydroxyphenyl)-2-[(Z)-3-(3,4-dihydroxyphenyl)acryloyl]oxy-propionic acid	109.38	0.35
MOL007140	(Z)-3-[2-[(E)-2-(3,4-dihydroxyphenyl)vinyl]-3,4-dihydroxy-phenyl]acrylic acid	88.54	0.26
MOL007141	salvianolic acid g	45.56	0.61
MOL007142	salvianolic acid j	43.38	0.72
MOL007143	salvilenone I	32.43	0.23
MOL007145	salviolone	31.72	0.24
MOL007149	NSC 122421	34.49	0.28
MOL007150	(6S)-6-hydroxy-1-methyl-6-methylol-8,9-dihydro-7H-naphtho[8,7-g]benzofuran-10,11-quinone	75.39	0.46
MOL007151	Tanshindiol B	42.67	0.45
MOL007152	Przewaquinone E	42.85	0.45
MOL007154	tanshinone iia	49.89	0.4
MOL007155	(6S)-6-(hydroxymethyl)-1,6-dimethyl-8,9-dihydro-7H-naphtho[8,7-g]benzofuran-10,11-dione	65.26	0.45
MOL007156	tanshinone VI	45.64	0.3

Notes: OB, Oral Bioavailability; DL, Drug-Likeness; ADME, Absorption, Distribution, Metabolism, Excretion.

Table 2. GO functional enrichment table for Danshen in the treatment of HF and iron metabolism.

Types	Term	Count	Enrichment Score	*p* value
BP	response to nicotine	7	4.844933797	3.73×10^{-8}
BP	response to glucocorticoid	7	5.145466488	1.10×10^{-7}
BP	extrinsic apoptotic signaling pathway in absence of ligand	6	4.257211096	6.28×10^{-7}
BP	positive regulation of peptidyl-serine phosphorylation	7	5.145466488	1.08×10^{-6}
BP	response to muscle stretch	5	3.822972582	1.56×10^{-6}
BP	activation of cysteine-type endopeptidase activity involved in apoptotic process	7	4.257211096	1.73×10^{-6}
BP	cellular senescence	6	3.83324354	6.47×10^{-6}
BP	negative regulation of autophagy	6	4.257211096	9.06×10^{-6}
BP	positive regulation of non-canonical NF-kappaB signal transduction	6	3.153129541	1.44×10^{-5}
CC	nucleoplasm	45	6.770523464	3.58×10^{-10}
CC	nucleus	54	6.770523464	1.16×10^{-8}
CC	receptor complex	10	2.339313467	6.07×10^{-7}
CC	chromatin	19	4.410314366	2.10×10^{-6}
CC	cytosol	46	6.770523464	4.27×10^{-6}
CC	transcription regulator complex	9	4.410314366	1.21×10^{-5}
CC	cytoplasm	44	6.770523464	4.68×10^{-5}
CC	cell surface	12	2.47850866	1.32×10^{-4}
CC	membrane raft	6	2.47850866	0.002309073
CC	RNA polymerase II transcription regulator complex	5	4.410314366	0.00231675
MF	nuclear receptor activity	9	5.295334913	1.55×10^{-10}
MF	nuclear receptor activity	9	3.779701442	1.55×10^{-10}
MF	estrogen response element binding	6	5.295334913	1.61×10^{-9}
MF	steroid binding	7	5.295334913	6.22×10^{-9}
MF	nuclear steroid receptor activity	5	5.295334913	3.82×10^{-6}
MF	zinc ion binding	17	3.779701442	4.02×10^{-6}
MF	heme binding	8	2.797217185	8.65×10^{-6}
MF	transcription cis-regulatory region binding	9	3.779701442	2.00×10^{-5}
MF	transcription coactivator binding	5	5.295334913	7.67×10^{-5}
MF	DNA-binding transcription activator activity, RNA polymerase II-specific	11	5.295334913	1.09×10^{-4}

GO, Gene Ontology; BP, biological processes; CC, cellular components; MF, molecular functions.

3.3 Construction of a Protein-Protein Interaction Network

The interaction data of the common targets for Danshen's treatment of HF and iron metabolism in the STRING database were used to obtain the overlapping gene PPI network diagram (Fig. 3). There were 92 nodes and 1543 edges. The PPI network diagram into Cytoscape 3.9.1 software and the MCC algorithm in the cytoHubba plugin was used to identify the top 10 most significant hub genes (Fig. 4).

Table 3. KEGG functional enrichment table for Danshen in the treatment of HF and iron metabolism.

Term	Enrichment Score	p value	Count
Endocrine resistance	9.835259674	3.38×10^{-17}	18
Hepatitis B	9.835259674	3.88×10^{-17}	21
Bladder cancer	9.835259674	2.00×10^{-15}	13
Platinum drug resistance	9.809474273	7.85×10^{-15}	15
IL-17 signaling pathway	5.302992243	1.10×10^{-14}	16
Human T-cell leukemia virus 1 infection	9.835259674	1.95×10^{-14}	21
Kaposi sarcoma-associated herpesvirus infection	9.835259674	2.31×10^{-14}	20
Human cytomegalovirus infection	9.835259674	2.53×10^{-14}	21
AGE-RAGE signaling pathway in diabetic complications	5.302992243	2.83×10^{-14}	16
Epstein-Barr virus infection	9.835259674	4.41×10^{-14}	20
Hepatitis C	9.835259674	1.25×10^{-13}	18
TNF signaling pathway	5.302992243	3.44×10^{-13}	16
Breast cancer	9.835259674	5.96×10^{-13}	17
Cellular senescence	9.835259674	1.50×10^{-12}	17
Colorectal cancer	9.835259674	1.57×10^{-12}	14
Toxoplasmosis	7.21390789	2.24×10^{-12}	15
Measles	9.835259674	3.48×10^{-12}	16
T cell receptor signaling pathway	5.302992243	8.39×10^{-12}	15
Relaxin signaling pathway	5.302992243	2.02×10^{-11}	15
Apoptosis	9.835259674	3.74×10^{-11}	15

KEGG, Kyoto Encyclopedia of Genes and Genomes.

3.4 GO Functional Enrichment

The DAVID database was used to perform GO functional analysis of the common targets of Danshen in the treatment of HF and iron metabolism. In terms of BP (Biological Process), select the top 10 ranked entries, which mainly involve cellular response to glucocorticoids, cellular response to nicotine, and extrinsic apoptotic signaling pathway in the absence of ligand. For CC (Cellular Component), select the top 10 ranked entries, which mainly include nucleoplasm, nucleus, and receptor complexes. For MF (Molecular Function), select the top 10 ranked entries, which mainly involve nuclear receptor activity, estrogen response element binding, and steroid binding, among others. The above results were input into the Bioinformatics website (http://www.bioinformatics.com.cn), and bubble charts for BP, CC, and MF were generated (see Fig. 5, Table 2).

3.5 KEGG Pathway Enrichment Analysis

The DAVID database was used to perform KEGG functional enrichment analysis of the common targets of Danshen in the treatment of HF and iron metabolism. The top 20 most significantly enriched pathways ($p < 0.01$) were selected, which mainly included pathways related to cellular senescence, apoptosis, AGE-RAGE, TNF, and IL-17 signaling. The results are shown in Fig. 6 and Table 3.

3.6 The Impact of Danshen on Liver Tissue Fibrosis

Comparison of HF histopathology among the groups: In the normal group, the liver lobule structure was intact, hepatocytes were neatly arranged, and there was no evidence of hepatocyte degeneration, necrosis, inflammatory cell infiltration, or fibrous cord formation. In the model group, the liver lobule structure was significantly disrupted with blurred boundaries, disordered cell cords, swollen hepatocytes, and cytoplasmic steatosis. Compared with the model group, the Danshen high-dose group showed a relatively intact liver lobule structure and cell morphology, with improved HF, reduced fibrous cords, and decreased degrees of cellular edema, necrosis, and steatosis. Compared with the model group, the Danshen low-dose group did not show significant pathological changes in tissue, with multiple pseudo-lobules, and cells exhibited varying degrees of edema, necrosis, inflammatory reactions, and steatosis. See Fig. 7.

3.7 The Impact of Danshen on HF Marker Proteins

Western blot results showed that compared with the blank group, the expression of IL-6, P-JAK2, and TGF-β1 proteins in the liver of the model group rats was significantly increased ($p < 0.05$), while the expression of IL-6, P-JAK2, P-STAT-3, and TGF-β1 in the Danshen intervention group was lower than that in the model group, especially in the high-dose Danshen group, where there was a significant downward trend ($p < 0.05$). High-dose Danshen significantly inhibited the expression of IL-6 and TGF-β1, and suppressed the phosphorylation of JAK2 and STAT3 (P-JAK2, P-STAT-3) in CCl4-induced HF model rats ($p < 0.05$), whereas the total protein levels of JAK2 and STAT-3 remained unchanged. The effect of low-dose Danshen was not significant ($p > 0.05$). See Fig. 8.

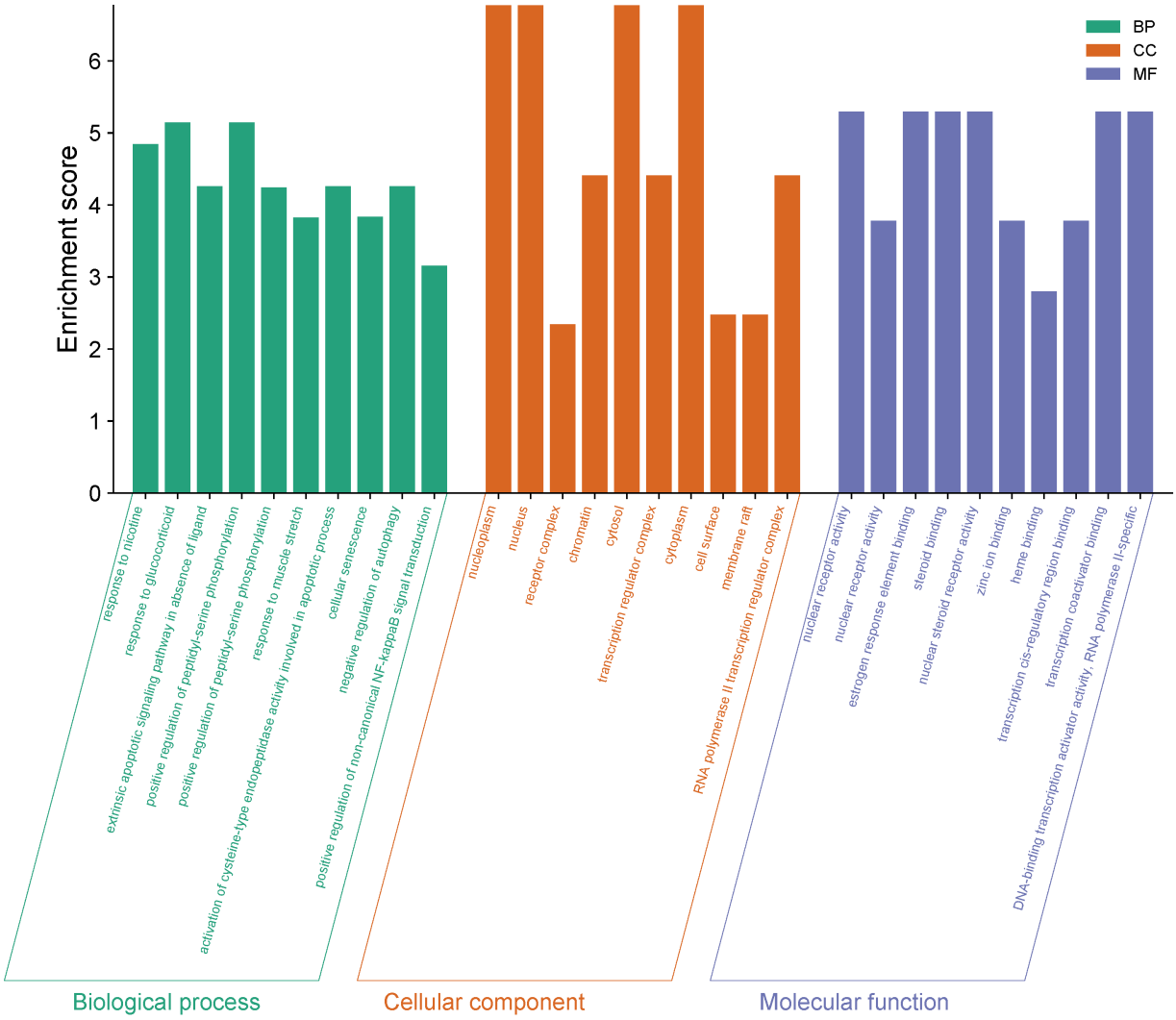

Fig. 5. GO functional enrichment bar chart for Danshen for the treatment of HF and iron metabolism. GO, Gene Ontology.

3.8 The Determination of Danshen's Effect on Blood Iron Metabolism Indicators

To further determine the occurrence of ferroptosis, serum Fe^{2+}, serum ferritin (SF), TRF, type III procollagen (PcIII), and hydroxyproline (HyP) levels were measured. The results showed that (see Fig. 9): compared with the blank group, the levels of Fe^{2+} and TRF in the serum of the model group were significantly decreased, while the levels of SF, PcIII, and HyP were significantly increased ($p < 0.05$). The Danshen intervention group showed an opposite trend to that of the model group in the levels of Fe^{2+}, TRF, SF, PcIII, and HyP, especially in the high-dose Danshen group, where the levels of Fe^{2+} and TRF were significantly increased, and the levels of SF, PcIII, and HyP were markedly decreased ($p < 0.05$). It can be seen that high-dose Danshen can promote an increase in blood Fe^{2+} and TRF concentrations and simultaneously decrease the concentrations of SF, PcIII, and HyP in CCl_4-induced HF model rats.

At the level of iron metabolism, a significant increase in blood Fe^{2+} and TRF levels indicates the restoration of normal iron utilization and storage in the body.

3.9 Danshen Attenuates Ferroptosis and Oxidative Stress in Hepatic Fibrosis

To determine whether Danshen ameliorates liver fibrosis through the ferroptosis pathway, we measured serum MDA and GSH levels and hepatic GPX4 protein expression (see Fig. 10). MDA, the core oxidative stress product of HF tissue, was significantly elevated in serum, while Danshen attenuated this increase. GSH, the antioxidant stress marker of HF tissue, was significantly decreased, while Danshen ameliorated this decline. Western blot analysis revealed significantly decreased GPX4 protein expression in fibrotic liver tissue, which was reversed by Danshen intervention; high-dose treatment restored GPX4 levels to near-normal. These findings demonstrate that Danshen ameliorates fibrotic liver injury by inhibiting ferroptosis-related pathways and suppressing oxidative stress.

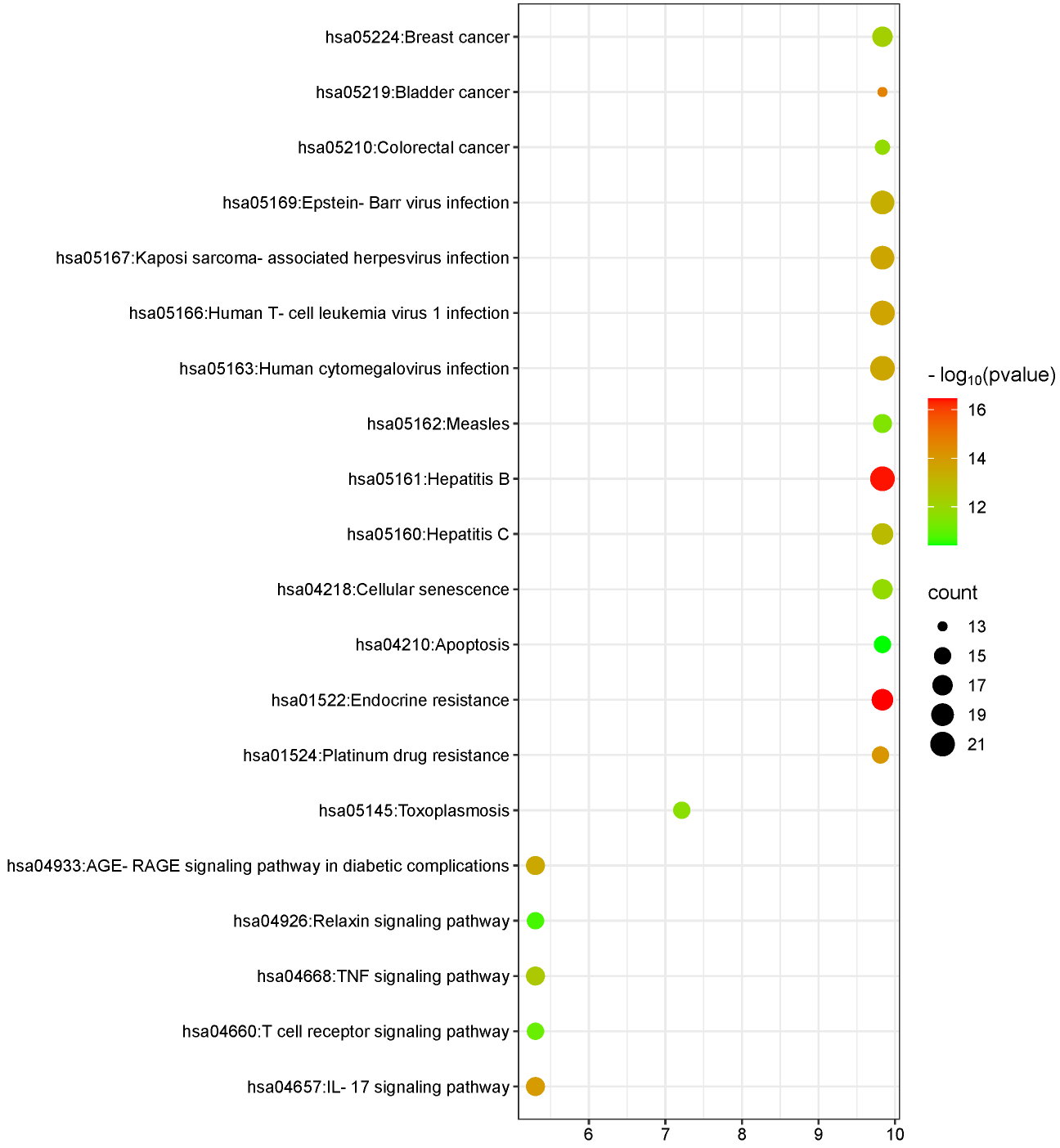

Fig. 6. KEGG pathway enrichment analysis bubble chart (the size of the bubbles in the chart represents the number of genes annotated in the corresponding entries, and the color of the bubbles corresponds to the corrected *p*-value). KEGG, Kyoto Encyclopedia of Genes and Genomes.

4. Discussion

This study establishes a mechanistic framework wherein Danshen ameliorates CCl_4-induced hepatic fibrosis through coordinated suppression of the IL-6/JAK/STAT3 inflammatory axis, restoration of iron homeostasis, and inhibition of ferroptosis. By integrating network pharmacology with experimental validation, we demonstrate that Danshen's therapeutic effects extend beyond conventional anti-inflammatory actions to encompass a novel "inflammation-iron-ferroptosis" regulatory network.

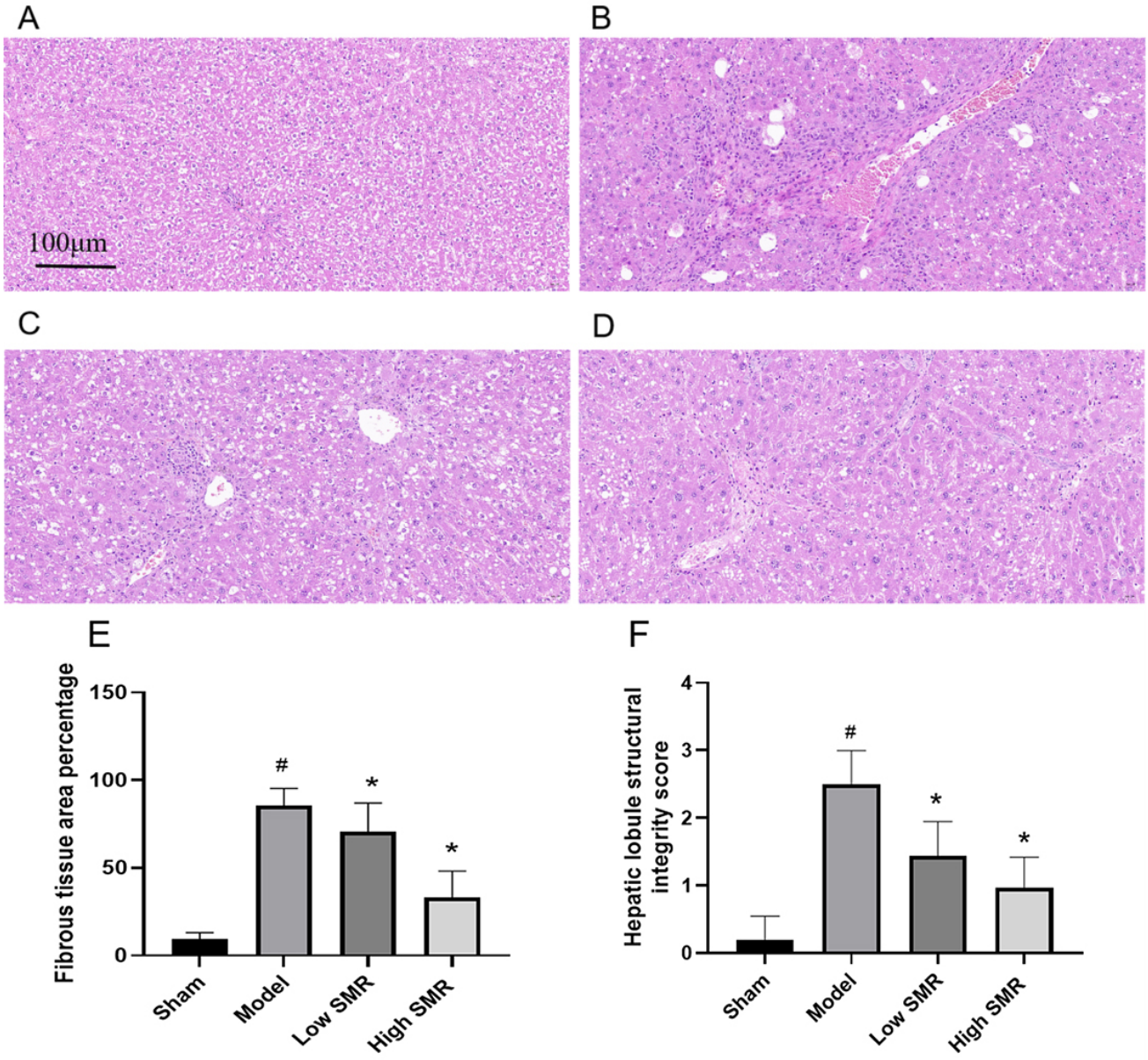

Fig. 7. The Impact of Danshen on liver tissue fibrosis. Effect of Danshen on liver tissue fibrosis: (A) sham group; (B) model group; (C) Danshen low-dose group; and (D) Danshen high-dose group. Scale bar = 100 μm. Percentage of fibrous tissue area (E), hepatic lobule structural integrity score (F). $^{\#}p < 0.05$ vs. the Sham group; $*p < 0.05$ vs. the Model group. Data are presented as mean ± standard error of the mean (SEM) (n = 3). $p < 0.05$ indicates statistical significance.

4.1 Network Pharmacology-Guided Target Selection Validated Experimentally

Our computational analysis identified 92 nodes at the intersection of Danshen, hepatic fibrosis, and iron metabolism, with JAK2/STAT3 emerging as top-ranking hub genes (Figs. 2,3,4). The significant enrichment of AGE-RAGE, TNF, and IL-17 pathways (Fig. 6) aligns with established fibrogenic mechanisms, while the prominence of "cellular senescence" and "apoptosis" pathways reflects the pleiotropic nature of Danshen's bioactive compounds. Notably, tanshinone IIA and cryptotanshinone—key diterpenoids exhibiting OB ≥30% and DL ≥0.18 (Table 1)-have been previously implicated in STAT3 inhibition and ferroptosis modulation [11,12]. The concordance between our *in silico* predictions and experimental data underscores the utility of network pharmacology for hypothesis generation in complex herbal medicine research.

4.2 IL-6/JAK/STAT3 as a Dual-Function Hub Integrating Inflammation and Iron Metabolism

The JAK/STAT3 pathway represents a critical convergence point for inflammatory and iron-regulatory signals in hepatic fibrosis [13]. Our data demonstrate that CCl_4-

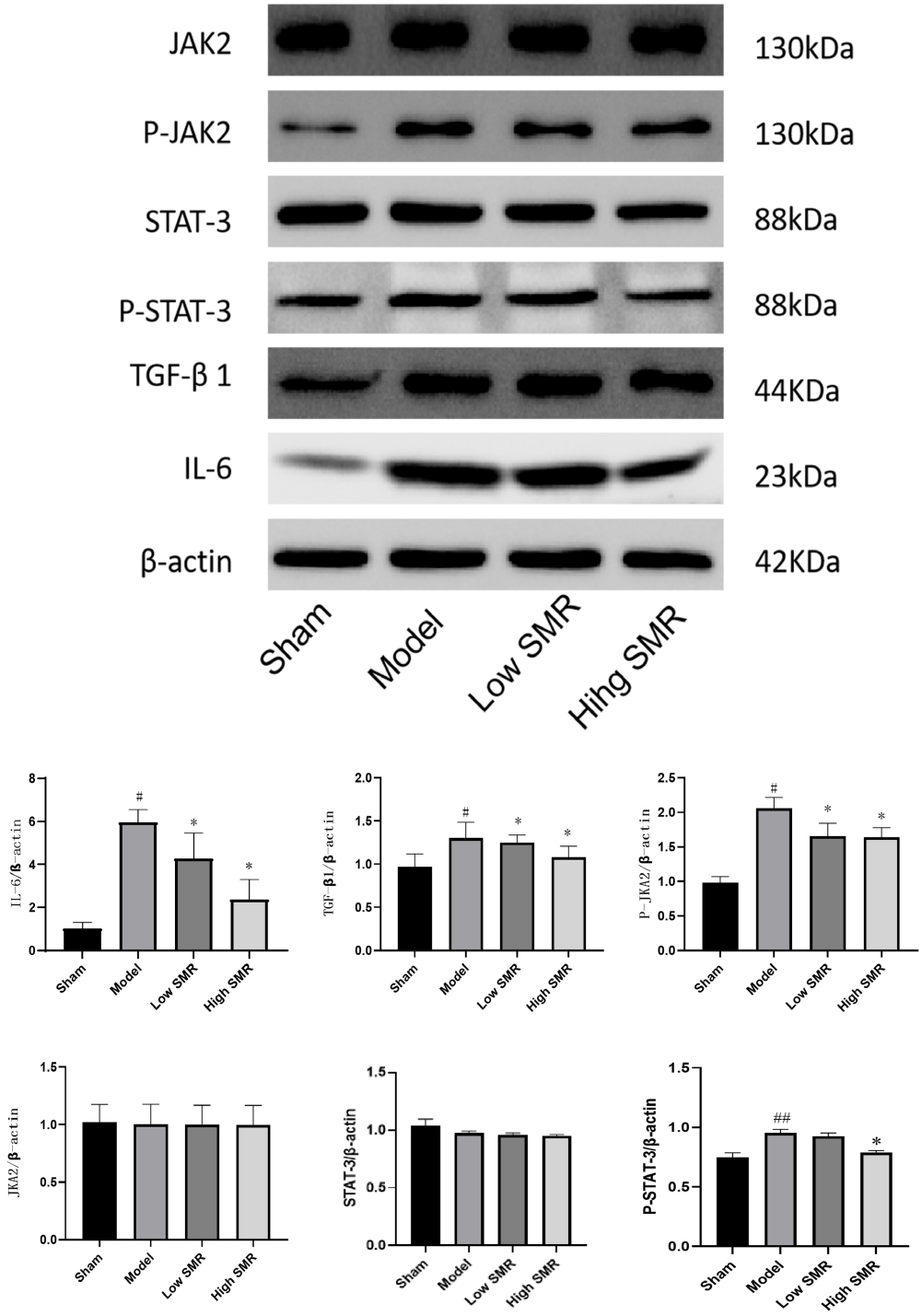

Fig. 8. The effect of Danshen on the proteins JAK2, P-JAK2, STAT3, P-STAT3, TGF-β1, and IL-6 in liver fibrotic tissue. $^{\#}p < 0.05$, $^{\#\#}p < 0.01$ vs. the Sham group; $^{*}p < 0.05$ vs. the Model group. Data are presented as mean $\pm$ standard error of the mean (SEM) (n = 3). $p < 0.05$ indicates statistical significance. JAK2, Janus kinase 2; P-JAK2, Phosphorylated Janus kinase 2; STAT3, Signal transducer and activator of transcription 3; P-STAT3, Phosphorylated Signal transducer and activator of transcription 3; TGF-β1, Transforming growth factor beta 1; IL-6, Interleukin-6.

induced fibrosis is characterized by IL-6 overexpression and STAT3 hyperphosphorylation, consistent with HSC activation and hepcidin-mediated iron sequestration [14]. Danshen dose-dependently suppressed IL-6 expression and STAT3 phosphorylation while preserving total STAT3 protein levels (Fig. 8), suggesting targeted modulation rather

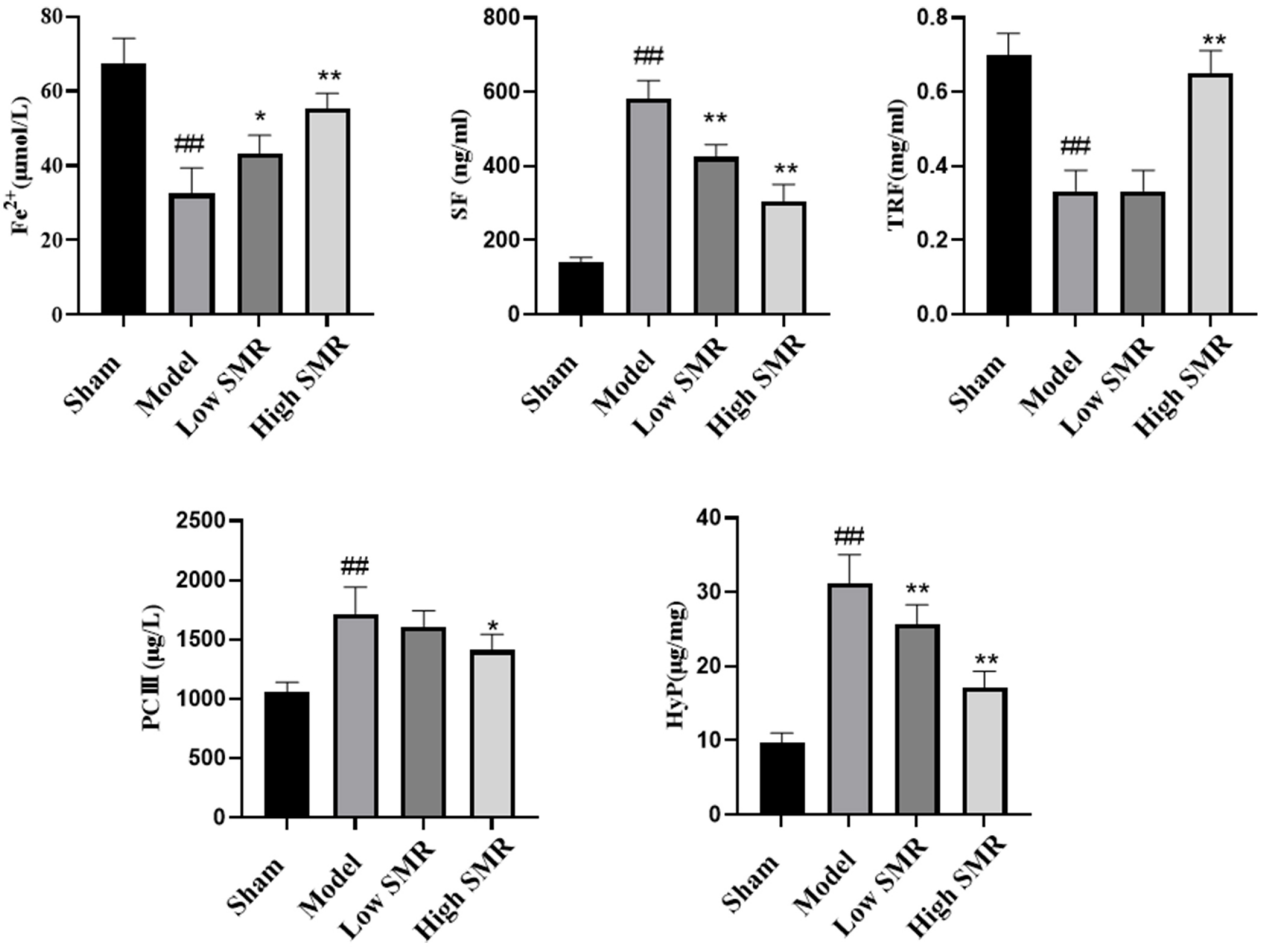

Fig. 9. Effect of danshen on blood Fe^{2+}, SF, TRF, PcIII, and HyP in HF rats. $^{\#\#}p < 0.01$ vs. the Sham group; $^{*}p < 0.05$, $^{**}p < 0.01$ vs. the Model group. Data are presented as mean ± standard error of the mean (SEM) (n = 3). $p < 0.05$ indicates statistical significance. SF, ferritin; TRF, transferrin; PcIII, type III procollagen; HyP, hydroxyproline.

than non-specific cytotoxicity. This is mechanistically significant because: (1) IL-6 is a master regulator of hepcidin transcription via STAT3 binding to the HAMP promoter [15]; (2) STAT3-driven hepcidin elevation impairs iron export via ferroportin degradation, creating a hypoxic microenvironment that perpetuates fibrogenesis [16]. By interrupting this feedforward loop, Danshen restores iron bioavailability, as evidenced by increased serum Fe^{2+}, transferrin (TRF) and decreased ferritin (SF) (Fig. 9). The observed 1.8-fold elevation in TRF is particularly noteworthy, as transferrin not only facilitates iron delivery but also acts as an antioxidant by sequestering free iron that would otherwise catalyze Fenton reactions [17].

4.3 Ferroptosis Inhibition: A Novel Anti-Fibrotic Mechanism of Danshen

Our data reveal that CCl_4-induced fibrosis produces a ferroptosis-permissive environment marked by GPX4 downregulation, GSH depletion, and MDA accumulation (Fig. 10), corroborating recent reports linking iron metabolism dysfunction to lipid peroxidation-driven cell death in chronic liver disease [18,19]. Danshen's restoration of GPX4 expression to near-normal levels represent a critical intervention point, as GPX4 is the sole enzyme capable of detoxifying membrane phospholipid hydroperoxides (PLOOHs) [20]. The reciprocal changes in MDA and GSH-core oxidative stress products and the primary GPX4 cofactor, respectively-demonstrate that Danshen reconstitutes the entire GPX4-GSH antioxidant axis. This finding resonates with recent observations that tanshinones can activate Nrf2, the transcriptional master regulator of GPX4 and GCLM (GSH synthesis) [21,22]. Importantly, our study places ferroptosis within the broader JAK/STAT signaling context: STAT3 activation transcriptionally represses Nrf2, creating a vicious cycle of oxidative stress [23]; Danshen's dual inhibition of STAT3 and restoration of GPX4-GSH likely disrupts this reciprocal inhibition.

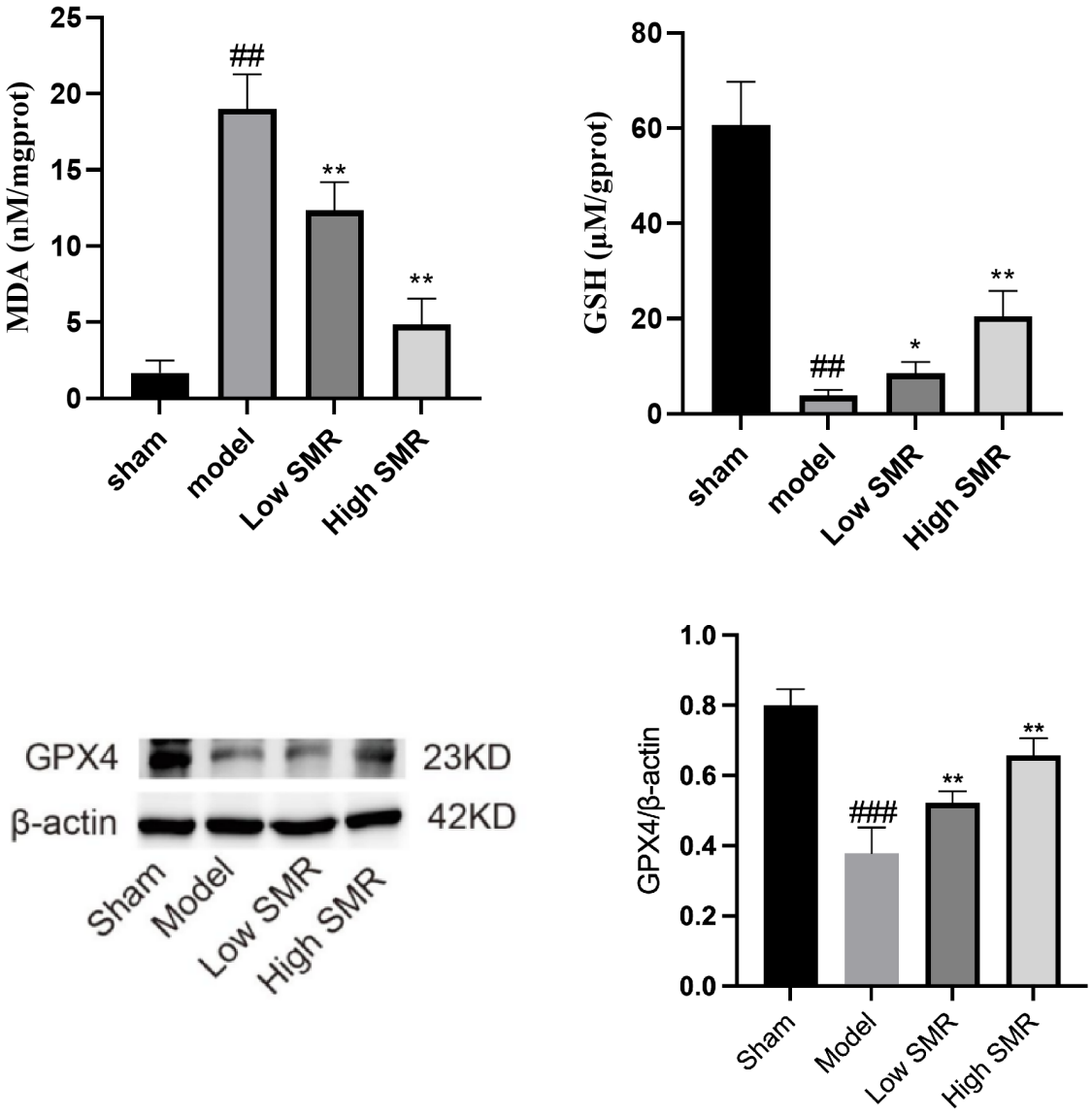

Fig. 10. Effects of Danshen on serum MDA and GSH levels and hepatic GPX4 protein expression in liver fibrotic tissue. $^{\#\#}p < 0.01$, $^{\#\#\#}p < 0.001$ vs. the Sham group; $^{*}p < 0.05$, $^{**}p < 0.01$ vs. the Model group. Data are presented as mean ± standard error of the mean (SEM) (n = 3). $p < 0.05$ indicates statistical significance. MDA, malondialdehyde; GSH, glutathione; GPX4, glutathione peroxidase 4.

4.4 The "Iron-Inflammation" Negative Feedback Loop: A Unifying Hypothesis

We propose a novel feedback mechanism wherein Danshen-induced normalization of iron metabolism reinforces anti-fibrotic efficacy (Fig. 9). Elevated bioavailable Fe^{2+} satisfies the requirement of prolyl hydroxylases for proper collagen cross-linking, reducing abnormal matrix deposition [24]. Simultaneously, increased intracellular iron may suppress IL-6 transcription via ROS-dependent inhibition of NF-κB signaling, or alternatively, promote IL-6 expression through iron-induced oxidative stress, depending on the cellular context and iron concentration, creating a stable anti-inflammatory state [25]. This "iron-inflammation" crosstalk, mediated through the JAK/STAT-GPX4 axis, represents a multi-dimensional therapeutic target that distinguishes Danshen from single-target anti-fibrotics.

4.5 Limitations and Future Directions

While our integrated approach provides compelling evidence, several limitations warrant acknowledgment. First, the mechanistic validation remains at the protein expression level; functional indispensability of the JAK/STAT axis should be confirmed using specific inhibitors (e.g., Ruxolitinib) or hepatocyte-specific Stat3 knockout mice. Second, although we demonstrate GPX4 restoration, direct

evidence that Danshen inhibits ferroptosis requires validation with GPX4 pharmacological inhibitors (RSL3/ML162) or conditional Gpx4 knockout models to establish causal dependency. Third, our study focused on male rats; sex-specific differences in iron metabolism and ferroptosis sensitivity necessitate future investigations in female cohorts [26]. Fourth, the network pharmacology analysis relied on databases with inherent annotation biases; experimental validation of additional hub genes (e.g., STAT1, ACVR1) would provide a more comprehensive understanding of Danshen's polypharmacology. Finally, translating these findings to clinical practice requires multi-center, double-blind trials evaluating Danshen's effects on serum PCIII, transient elastography, and patient-reported outcomes.

5. Conclusions

This study demonstrates that Danshen attenuates CCl_4-induced hepatic fibrosis by downregulating the IL-6/JAK/STAT3 inflammatory axis, restoring iron homeostasis, and inhibiting ferroptosis through GPX4-GSH pathway activation. The identification of a "JAK/STAT-iron-ferroptosis" regulatory network provides a novel mechanistic framework for Danshen's anti-fibrotic effects and highlights therapeutic potential for dual-targeting inflammation and iron-dependent cell death. Future studies leveraging genetic models and clinical translation will further solidify these findings and establish Danshen as a viable multimodal therapy for hepatic fibrosis.

Availability of Data and Materials

All data reported in this paper will also be shared by the lead contact upon request.

Author Contributions

WO are responsible for the conception and design of articles, collection and collation of research materials, and drafting the manuscript. CL are responsible for the design the research study, review of the manuscript, overall supervision and Financial support. Both authors contributed to editorial changes in the manuscript. Both authors read and approved the final manuscript. Both authors have participated sufficiently in the work and agreed to be accountable for all aspects of the work.

Ethics Approval and Consent to Participate

The animal study protocol was approved by the Experimental Animal Ethics Committee of Haikou Affiliated Hospital of Central South University XiangYa School of Medicine (i.e., Haikou people's Hospital). The ethical lot number: 2020- (Lunshen) -247. All experimental procedures were conducted in accordance with the relevant guidelines and regulations for the care and use of laboratory animals, including but not limited to the National Institutes of Health Guide for the Care and Use of Laboratory Animals. All efforts were made to minimize animal suffering and to reduce the number of animals used.

Acknowledgment

We gratefully acknowledge the assistance and instruction from Haikou Affiliated Hospital of Central South University XiangYa School of Medicine and Hainan Medical University.

Funding

This research was funded by Hainan Provincial Natural Science Foundation of China, grant number 821MS0846.

Conflict of Interest

The authors declare no conflict of interest.

References

[1] Sun Y, Yuan X, Hu Z, Li Y. Harnessing nuclear receptors to modulate hepatic stellate cell activation for liver fibrosis resolution. Biochemical Pharmacology. 2025; 232: 116730. https://doi.org/10.1016/j.bcp.2024.116730.

[2] Zamani M, Alizadeh-Tabari S, Ajmera V, Singh S, Murad MH, Loomba R. Global Prevalence of Advanced Liver Fibrosis and Cirrhosis in the General Population: A Systematic Review and Meta-analysis. Clinical Gastroenterology and Hepatology: the Official Clinical Practice Journal of the American Gastroenterological Association. 2025; 23: 1123–1134. https://doi.org/10.1016/j.cgh.2024.08.020.

[3] Czaja AJ. Hepatic inflammation and progressive liver fibrosis in chronic liver disease. World Journal of Gastroenterology. 2014; 20: 2515–2532. https://doi.org/10.3748/wjg.v20.i10.2515.

[4] Berumen J, Baglieri J, Kisseleva T, Mekeel K. Liver fibrosis: Pathophysiology and clinical implications. WIREs Mechanisms of Disease. 2021; 13: e1499. https://doi.org/10.1002/wsbm.1499.

[5] Ge T, Wang Y, Han Y, Bao X, Lu C. Exploring the Updated Roles of Ferroptosis in Liver Diseases: Mechanisms, Regulators, and Therapeutic Implications. Cell Biochemistry and Biophysics. 2025; 83: 1445–1464. https://doi.org/10.1007/s12013-024-01611-3.

[6] Lin L, Li X, Li Y, Lang Z, Li Y, Zheng J. Ginsenoside Rb1 induces hepatic stellate cell ferroptosis to alleviate liver fibrosis via the BECN1/SLC7A11 axis. Journal of Pharmaceutical Analysis. 2024; 14: 100902. https://doi.org/10.1016/j.jpha.2023.11.009.

[7] Wu J, Wang Y, Jiang R, Xue R, Yin X, Wu M, *et al*. Ferroptosis in liver disease: new insights into disease mechanisms. Cell Death Discovery. 2021; 7: 276. https://doi.org/10.1038/s41420-021-00660-4.

[8] Li Z, Zhu JF, Ouyang H. Progress on traditional Chinese medicine in improving hepatic fibrosis through inhibiting oxidative stress. World Journal of Hepatology. 2023; 15: 1091–1108. https://doi.org/10.4254/wjh.v15.i10.1091.

[9] Li WQ, Liu WH, Qian D, Liu J, Zhou SQ, Zhang L, *et al*. Traditional Chinese medicine: An important source for discovering candidate agents against hepatic fibrosis. Frontiers in Pharmacology. 2022; 13: 962525. https://doi.org/10.3389/fphar.2022.962525.

[10] Jung I, Kim H, Moon S, Lee H, Kim B. Overview of *Salvia miltiorrhiza* as a Potential Therapeutic Agent for Various Diseases:

An Update on Efficacy and Mechanisms of Action. Antioxidants (Basel, Switzerland). 2020; 9: 857. https://doi.org/10.3390/antiox9090857.

[11] Cui C, Yang F, Li Q. Post-Translational Modification of GPX4 is a Promising Target for Treating Ferroptosis-Related Diseases. Frontiers in Molecular Biosciences. 2022; 9: 901565. https://doi.org/10.3389/fmolb.2022.901565.

[12] Li X, Wang TX, Huang X, Li Y, Sun T, Zang S, *et al*. Targeting ferroptosis alleviates methionine-choline deficient (MCD)-diet induced NASH by suppressing liver lipotoxicity. Liver International: Official Journal of the International Association for the Study of the Liver. 2020; 40: 1378–1394. https://doi.org/10.1111/liv.14428.

[13] Pellicoro A, Ramachandran P, Iredale JP, Fallowfield JA. Liver fibrosis and repair: immune regulation of wound healing in a solid organ. Nature Reviews. Immunology. 2014; 14: 181–194. https://doi.org/10.1038/nri3623.

[14] Wang Y, Hu J, Wu S, Fleishman JS, Li Y, Xu Y, *et al*. Targeting epigenetic and posttranslational modifications regulating ferroptosis for the treatment of diseases. Signal Transduction and Targeted Therapy. 2023; 8: 449. https://doi.org/10.1038/s41392-023-01720-0.

[15] Ganz T, Nemeth E. Hepcidin and iron homeostasis. Biochimica et Biophysica Acta. 2012; 1823: 1434–1443. https://doi.org/10.1016/j.bbamcr.2012.01.014.

[16] Besson-Fournier C, Latour C, Kautz L, Bertrand J, Ganz T, Roth MP, *et al*. Induction of activin B by inflammatory stimuli up-regulates expression of the iron-regulatory peptide hepcidin through Smad1/5/8 signaling. Blood. 2012; 120: 431–439. https://doi.org/10.1182/blood-2012-02-411470.

[17] Gomme PT, McCann KB, Bertolini J. Transferrin: structure, function and potential therapeutic actions. Drug Discovery Today. 2005; 10: 267–273. https://doi.org/10.1016/S1359-6446(04)03333-1.

[18] Zhang Z, Yao Z, Wang L, Ding H, Shao J, Chen A, *et al*. Activation of ferritinophagy is required for the RNA-binding protein ELAVL1/HuR to regulate ferroptosis in hepatic stellate cells. Autophagy. 2018; 14: 2083–2103. https://doi.org/10.1080/15548627.2018.1503146.

[19] Sun S, Shen J, Jiang J, Wang F, Min J. Targeting ferroptosis opens new avenues for the development of novel therapeutics. Signal Transduction and Targeted Therapy. 2023; 8: 372. https://doi.org/10.1038/s41392-023-01606-1.

[20] Yang WS, Stockwell BR. Ferroptosis: Death by Lipid Peroxidation. Trends in Cell Biology. 2016; 26: 165–176. https://doi.org/10.1016/j.tcb.2015.10.014.

[21] Feng F, Cheng P, Xu S, Li N, Wang H, Zhang Y, *et al*. Tanshinone IIA attenuates silica-induced pulmonary fibrosis via Nrf2-mediated inhibition of EMT and TGF-β1/Smad signaling. Chemico-biological Interactions. 2020; 319: 109024. https://doi.org/10.1016/j.cbi.2020.109024.

[22] Suzuki T, Yamamoto M. Stress-sensing mechanisms and the physiological roles of the Keap1-Nrf2 system during cellular stress. The Journal of Biological Chemistry. 2017; 429: 1467–1486. https://doi.org/10.1074/jbc.R117.800169.

[23] Alnajem A, Al-Maghrebi M. The Regulatory Effects of JAK2/STAT3 on Spermatogenesis and the Redox Keap1/Nrf2 Axis in an Animal Model of Testicular Ischemia Reperfusion Injury. Cells. 2023; 12: 2292. https://doi.org/10.3390/cells12182292.

[24] Myllyharju J. Prolyl 4-hydroxylases, the key enzymes of collagen biosynthesis. Matrix Biology: Journal of the International Society for Matrix Biology. 2003; 22: 15–24. https://doi.org/10.1016/s0945-053x(03)00006-4.

[25] Lee J, Hyun DH. The Interplay between Intracellular Iron Homeostasis and Neuroinflammation in Neurodegenerative Diseases. Antioxidants. 2023; 12: 918. https://doi.org/10.3390/antiox12040918.

[26] He Z, Liu B, Xian Z, Gong A, Jia X. Ferroptosis in Autoimmune Diseases: Research Advances and Therapeutic Strategies. International Journal of Molecular Sciences. 2025; 26: 10449. https://doi.org/10.3390/ijms262110449.